

Shi W, Atlar M, Norman R, Aktas B, Turkmen S.

[Numerical optimization and experimental validation for a tidal turbine blade with leading-edge tubercles.](#)

Renewable Energy 2016, 96(Part A), 42-55.

Copyright:

© 2016. This manuscript version is made available under the [CC-BY-NC-ND 4.0 license](#)

DOI link to article:

<http://dx.doi.org/10.1016/j.renene.2016.04.064>

Date deposited:

13/05/2016

Embargo release date:

03 May 2017



This work is licensed under a

[Creative Commons Attribution-NonCommercial-NoDerivatives 4.0 International licence](#)

**Numerical optimization and experimental validation for a
tidal turbine blade with leading-edge tubercles**

Weichao Shi^{*1}, Mehmet Atlar¹, Rosemary Norman¹, Batuhan Aktas¹, Serkan Turkmen¹

1 School of Marine Science and Technology, Newcastle University, UK

Corresponding Author:

Weichao Shi, w.shi6@newcastle.ac.uk

**School of Marine Science and Technology
Armstrong Building, Newcastle University
United Kingdom, NE1 7RU
Tel: 0044 (0)191 222 6726
Fax: 0044 (0)191 222 5491**

Abstract: Recently the leading-edge tubercles on the pectoral fins of humpback whales have attracted the attention of researchers who wish to exploit this feature in the design of turbine blades to improve the blade performance. The main objective of this paper is therefore to make a further investigation into this biomimetic design inspiration through a fundamental research study involving a hydrofoil section, which represents a straightened tidal turbine blade, with and without the leading-edge tubercles, using computational and experimental methods.

Firstly a computational study was conducted to optimise the design of the leading-edge tubercles by using commercial CFD code, ANSYS-CFX. Based on this study the optimum tubercle configuration for a tidal turbine blade with S814 foil cross-section was obtained and investigated further. A 3D hydrofoil model, which represented a “straightened” tidal turbine blade, was manufactured and tested in the Emerson Cavitation Tunnel of Newcastle University to investigate the effect of various tubercle options on the lift and drag characteristics of the hydrofoil. The experiments involved taking force measurements using a 3-component balance device and flow visualisation using a Particle Image Velocimetry (PIV) system. These tests revealed that the leading-edge tubercles may have significant benefits on the hydrodynamic performance of the hydrofoil in terms of an improved lift-to-drag ratio performance as well as reducing the tip vortex which is main cause of the undesirable end-effect of 3D foils. The study explores further potential benefits of the application of leading-edge tubercles on tidal turbine blades.

Keywords: Tidal turbine, Leading-edge tubercle, Foil tests, Computational Fluid Dynamics (CFD), Lift and drag measurements, Flow visualisations, Particle Image Velocimetry (PIV)

1 Introduction

The humpback whale is a species of giant marine mammal, ranging from 12~16m long. In spite of its large size this creature is unique in its ability to do athletic manoeuvres, especially in catching its prey, compared to other similarly sized marine mammals. Humpback whales utilize their unusually long pectoral fins to perform tight turns to drive a school of fish into a small circular zone so that they can swallow their prey all together. Close observation of their long fins indicates that the leading edges of these fins are not smooth, having some tubercles which are round shape protuberances [1, 2]. Wind tunnel tests showed that placing leading-edge tubercles on foils could improve the foil performance in terms of delayed stall and higher lift-to-drag ratio [3-8].

A number of numerical and experimental investigations has been conducted to understand the tubercle concept [8-12]. Some of these investigations indicated that the effects caused by the tubercles on the performance of a 2 dimensional (2D) foil and 3 dimensional (3D) foil are quite different [3, 5, 6, 9, 11, 13-15]. Studies on the 2D foils were more focused on the optimisation of the sinusoidal shape tubercle profiles defined by different parameters. Optimised tubercle profiles on these 2D sections could improve the lift coefficient curves further by maintaining the lift after the stall point. However this was at the cost of a reduction in the maximum lift coefficients since the drag coefficients were increased by these tubercles, at the same time. On the other hand, different performance characteristics have been reported based on the investigations with the leading-edge tubercles on 3D foils which are usually tip tapered like rudders, stabilizer fins, wings, flippers etc. The investigations with the 3D foils also claim the improvement of the lift coefficient curves by maintaining the lift beyond the stall point which is similar to the effect of tubercles on 2D foils. However, in addition to this, the performance regarding to the lift-to-drag ratio can be enhanced [6-8, 11, 16, 17].

Encouraged by the previous investigations into tubercle performance, especially for the 3D foil applications, an attempt was made recently to apply the tubercle concept to tidal turbine blades and scaled turbine models with different tubercle designs were tested in a towing tank [18]. Some performance improvement was demonstrated in this application even though the power coefficients achieved were not comparable to state-of-the-art levels due to various design and other issues developed during the tests. The blade with only a 1/3 of the span covered with tubercles displayed the best performance amongst the different ranges of the tubercle extensions over the blade span. Based on the results of this recent research it was thought that, there was a scope for further research and development in this field to improve the performance of a tidal turbine and demonstrate it in a validated manner.

The main objective of this study is therefore to make a further contribution to the understanding of the tubercle concept in the design of tidal turbine blades by using computational and experimental approaches. Within this framework, a fundamental investigation using a single 2D and 3D blade configuration is presented in this study. This is intended to achieve some basic understandings of the leading-edge tubercles on a straightened turbine blade prior to applying them to the real blades of a whole tidal turbine.

In the remainder of this paper, an optimization study is presented in Section 2 to optimise the main parameters of the leading-edge tubercles for a single blade with S814 cross-section profile by using the commercial CFD software, ANSYS-CFX. In this exercise a reference 2D foil

fitted with different sizes of tubercles was analysed to lead on to the design of a 3D foil with tubercles. Then a straightened 3D foil based on a tidal turbine blade with the same chord length distribution but with a constant pitch angle was designed by using the optimised tubercles and a physical model based on this design was tested in a cavitation tunnel as presented and discussed in Section 3 of the paper. Finally main conclusions obtained from the study are presented in Section 4.

2 Tubercle Design and Optimization

2.1 Description of Tubercle Design

The design study was based on a previous UK National research programme (EPSRC-RNET), in which a tidal turbine was designed based on the S814 profile cross-section from the NREL series, as shown in Figure 1 from Wang et al [19] who conducted an experimental investigation into the efficiency, slipstream wash, cavitation and noise characteristics of this turbine. The scaled turbine model is shown in Figure 2 as mounted on the open water dynamometer of the Emerson Cavitation Tunnel of Newcastle University. A representative and straightened version of this turbine blade, which is based on the S814 profile cross-section, was considered as the reference foil in this study to apply the tubercle concept.

The investigation into the optimisation of the tubercle profiles was initiated by systematically changing the Height (H) and the Wavelength (W) of these protrusions based on the sinusoidal form of their shapes. Two sets of tubercle designs were simulated with two different heights which were assumed 5% and 10% of the foil chord length (C) and combined with ten wavelength arrangements varying from 0.1C to 1C in 0.1C increments. The definitions of these parameters are shown in Figure 3.

2.2 Numerical Method and Validation

Before investigating the effect of the designed tubercles on the foil performance, the foil test data available from Ohio State University was used to validate the CFD model [20, 21]. According to the previous 2D foil studies [5, 6, 8, 11], the tubercles were found to be beneficial when the foil was under stall or near stall conditions. However the simulation of a foil performance under stall conditions was a challenging case in CFD simulations [22, 23]. Therefore the establishment of a reliable CFD model, in terms of the turbulence modelling, effective mesh generation, etc., would be critical for the simulations as discussed in the next.

2.2.1 Turbulence Model

For the optimisation study presented here, a more computationally economical time independent steady state RANS model was preferred. Industrially acknowledged and recommended K-epsilon and Shear Stress Transport (SST) turbulence models were investigated in the study [23].

2.2.2 Mesh Generation

Mesh quality for curved surfaces is another critical issue for CFD simulations. As a first attempt a structured mesh of around 1 million O-type elements was generated by the ANSYS-

MESHING module [23]. The value of the non-dimensional wall parameter, y^+ , was kept as 1 to ensure the required mesh quality within the boundary layer [22] and the growth ratio was limited to 1.08. The outer boundary was set at about 10 chord lengths away from the foil. Meanwhile newly developed Solution Adaptive Mesh technology was also used to adapt the mesh automatically based on the flow gradient [23]. This enabled more effective mesh distribution depending on the requirements.

Figure 4 shows the whole mesh and the details of the grid near the foil section before the solution adaptive mesh was processed. However after the process of solution mesh adaption, the number of elements became around 2.5 million or more which depended on the calculation cases. The mesh would be further refined automatically during the simulation itself, as shown in Figure 5.

2.2.3 Validation of CFD

Figure 6 shows the comparison of the CFD predictions for the experimental lift and drag coefficients of the Ohio State University foil. The CFD simulations were conducted using both K-epsilon and SST turbulence models by maintaining the chord length based Reynolds number at 10^6 . As shown in Figure 6, both CFD simulations with the two different turbulence models displayed very good agreement with the experiments up to a 10 deg of angle of attack (AOA) where the stall occurred. After the stall, the CFD predictions overestimated the lift coefficient especially using the K-epsilon turbulence model. However, when the CFD simulation with the SST turbulence model was combined with the solution adaptive mesh technique [22] the prediction was greatly improved, as shown in Figure 6. Similar comparisons are also shown for the drag coefficients. As shown in Figure 6, the predictions with the SST turbulence model combined with the solution adaptive technique show close agreement with the experimental data. Finally, the comparisons of the CFD predictions with the experimentally measured pressure distribution around the foil in stall condition are shown in Figure 7 and Figure 8 and again display very good correlations. Therefore the SST turbulence model with the solution adaptive mesh was adopted for the analysis of the flow.

2.3 Optimization Result and Analysis

Using the validated CFD model, the lift coefficients of the foil with the S814 profile cross-section and sinusoidal tubercles of differing parameters were simulated. As shown in Figure 9 and Figure 10, the tubercles on 2D foils maintained higher lift coefficients in the post-stall region ($20^\circ \sim 40^\circ$) while they also reduced the maximum lift coefficient. Increasing the tubercle wavelengths brought the lift coefficients of the foil with the leading-edge tubercles closer to the lift coefficients of the reference or “baseline” foil with the smooth leading edge i.e. without tubercles. However reducing the wavelengths increased the lift at higher angles of attacks while reducing the maximum value of the lift. By taking into account these trends, the foil having a sinusoidal form of tubercle with the height and wavelength of $H=0.1C$ and $W=0.5C$, respectively, was considered to be a good compromise from the performance point of view and was chosen for further analysis as a 3D foil.

Post analysis of the CFD simulation results of the cases, “Baseline” and the optimised “H-0.1, W-0.5”, under 15° are shown in Figure 11. The velocity iso-surfaces for the case where the velocity is equal to 50% of the incoming velocity, reveal the flow separation patterns and were plotted and coloured base on the pressure distribution. As shown in Figure 11, the flow pattern

around the foil was favourably affected by the presence of the tubercles as the flow appeared to be more attached to the foil surface following the crest of the tubercles whereas the baseline foil without tubercles displayed separated flow after the leading edge.

3 Foil Design and Test

Having conducted the CFD analysis on the 2D foil and validated the results, the next task was the design of a representative 3D foil with tubercles, based on an existing tidal turbine blade, and to conduct dedicated experiments to investigate the effect of tubercles on the hydrodynamic characteristics of this foil.

3.1 Foil Design and Manufacture

As reported in the open literature [6, 11] by previous researchers the effect of tubercles on the hydrodynamic performance of 2D and 3D foils was different and further evidence supporting this claim would be welcome as one of the natural outcomes of the present study. Therefore a 3D foil representing a turbine blade was designed and model tested in this section.

As stated in Section 2.1, the representative 3D foil was based on the blade of the tidal turbine designed by Wang et al [19]. However, while the foil had the same chord length distribution as the subject tidal turbine blade it had a constant pitch. Based on the limitations imposed by the testing section of the ECT, the span of the test foil was specified as 560mm. Considering the operating range of the tip speed ratios (TSRs), the range of the angles of attack (AOA) to be applied on the foil during the tests was specified to be 0° to 40° while the inflow velocities were selected as 2, 3 and 4m/s. Over this inflow velocity range, the reference Reynolds number (Re), which was described based on the chord length (150mm) of the foil at 0.7 radius, was varied from 0.3×10^6 to 0.6×10^6 . This was similar to the Re range for the turbine model that was used by Wang et al [19].

According to the optimisation task with the 2D foil presented in Section 2.3, the foil with the tubercles would display relatively the best performance when the height (H) and wavelength (W) of the tubercles were 0.1C and 0.5C, respectively. Hence approximately 8 sinusoidal tubercles with successive crests and troughs were evenly distributed along the leading edge.

Based on the above arrangement, the 3D foil was manufactured in two separate parts and then assembled. The first part was the interchangeable (or removable) leading-edge part of the foil while the second part was the remainder (i.e. main body) of the foil that also supported the whole foil structure. The interchangeable leading-edge was printed using a 3D printer in four segmented pieces from a liquid resin material, Stratasys Vero White Plus RGD835.

The interchangeable and segmented manufacture of the leading-edge profiles provided very useful flexibility for testing the different leading-edge arrangements as well as overcame the size limitation of the 3D printer. The main body of the foil was milled by CNC machine from a carbon fibre reinforced plastic (CFRP) to ensure that the structure would be strong enough and the deformation minimal. All the models with various combinations of the leading edge profiles are shown in Figure 12.

The main foil with five different leading-edge combinations, one of which was the smooth leading edge, was tested and corresponding hydrodynamic performances were compared to explore the effect of the four different tubercle arrangements on the foil performance. In order to classify the different leading-edge tubercle combinations, the reference foil with the smooth leading-edge section was represented by legend “0000” while the foil with the leading-edge tubercles covering the whole span was represented by “1111”. Other leading-edge combinations with partial tubercle applications were represented using legend “0001”, “0011” and “0111” for the 1/4, 1/2 and 3/4 coverage of the foil span by the tubercles from tip to root, respectively.

3.2 Experimental Setup

The experiments were conducted in the Emerson Cavitation Tunnel (ECT) at Newcastle University. The tunnel is a medium size propeller cavitation tunnel with a measuring section of 1219mm×806mm (width × height), as shown in Figure 13. The speed of the tunnel inflow varies between 0.5 to 8 m/s. Full details of the ECT and its further specifications can be found in reference [24].

The lift and drag performance of the test foil was the primary interest during the experiments as in many foil investigations. During the tests, the forces (X, Y) acting on the foil, which was suspended vertically from the upper lid in the mid-plane of the tunnel measuring section, were measured using a 3-component balance device. This device was a Cussons R102 balance which was specially designed and manufactured for the ECT to be mounted on the top lid of the tunnel using a height and angle adjustment mechanism. The test foil was mounted to the bottom plate of the 3-component balance to transfer the forces to the 3 load cells and a circular plate was fitted at the root of the blade to prevent the tunnel inflow entering into the cavity, where the balance was housed, as shown in Figure 14.

The measured lift and drag forces were represented by the following non-dimensional coefficients:

$$C_L = \frac{Lift}{\frac{1}{2}\rho V^2 A} \quad \text{Equation (1)}$$

$$C_D = \frac{Drag}{\frac{1}{2}\rho V^2 A} \quad \text{Equation (2)}$$

Where *Lift* is the measured lift of the foil which is perpendicular to the incoming flow; *Drag* is the measured drag of the foil which is aligned with the incoming flow; ρ is the density of the tunnel water, which was measured as 1004 kg/m³ using a density meter; *V* is the tunnel inflow velocity; *A* is the reference area of the foil which is assumed to be equal to the foil projected area, 0.0924 m².

All the measured data were gathered by a National Instruments data acquisition system and analysed instantaneously by LabVIEW. For each measurement point, 500,000 samples were

acquired at a 1 kHz sample rate and averaged to calculate the mean value. During the experiments, each test run was repeated three times for uncertainty analysis. The average results were then plotted and compared. The maximum values of CL and CD were 2.3% and 3.1%, respectively, with mean values of standard deviation of 1.1% and 1.0%, respectively. One example of the uncertainty analysis is presented in Figure 15.

In order to measure and analyse the flow field around the foil, a 2D particle image velocimetry (PIV) system was used, while some still photo images were also taken. The detailed technical specification of the PIV system used, which was a Dantec Dynamics Ltd product, is shown in Table 2. During the use of this system, the flow field was illuminated by the planar laser light sheet which was perpendicular to the hydrofoil and highly seeded flow field images were captured by the double framing high-speed CCD camera at a frequency of 500Hz and 0.0004s time interval. Throughout the measurements, 100 double frame image pairs needed to be captured, analysed and averaged to achieve a time-averaged velocity distribution. The adaptive PIV analysis was used for the 2D images from each camera with a grid size of 16x16 pixels. Afterwards, the results of these 100 velocity samples were averaged to achieve the final results.

3.3 Force Measurement Results and Analysis

3.3.1 Reynolds Number Effect

First of all, based on the above test set-up, the reference foil “0000” was tested at 2, 3 and 4m/s tunnel velocity to demonstrate the effect of Reynolds number (Re). Because of the practical limitations of the testing facility, a typical full-scale Re range for a tidal turbine, which often ranges from 10×10^6 to 30×10^6 based on the chord length at 0.7 radius, could not easily be met within the model scale test. In the current tests, the Re range was varied from 0.3×10^6 to 0.6×10^6 where the Re was described based on the reference chord length of 150mm at 0.7 radius. It is important that the Reynolds number effect has to be checked prior to any flow tests and certain precautions must be taken to improve the circumstances for very low Re cases.

Figure 16 shows the measured lift, drag and lift-to-drag ratio of the reference foil (i.e. Foil 0000) which are represented in terms of the associated coefficients as described in Section 3.2. In this figure the last character with an underscore bar in the legend used refers to the tunnel incoming velocity (e.g. 0000_2, where the tunnel velocity is 2 m/s). As shown in Figure 16, within the range of the Reynolds numbers tested, the slope and maximum value of lift coefficients decrease gradually with increasing Re. On the other hand, the drag coefficients are nearly identical for different values of Reynolds number. Thus, the lift-to-drag ratios of the reference foil with the smooth leading-edge are reduced with increasing Reynolds number.

The tests conducted for the reference foil (Foil “0000”) were repeated for Foil “1111” which had full leading-edge tubercles and the results are presented in Figure 17. As shown in Figure 17, unlike in the reference foil case, the lift coefficient of the foil with the leading-edge tubercles increases with the Reynolds number, particularly after a 14° angle of attack (AOA) for 2m/s and 3m/s flow speed. A large gap can be seen between the lift coefficients for 2m/s and 3m/s. There seemed to be a trend suggesting that the lift-to-drag ratio can be enhanced with increasing Reynolds number and hence the foil with the leading-edge tubercles may have a better performance at higher range of Reynolds number.

3.3.2 Performance Comparison between the Foils with and without Tubercles

Figure 18 shows the comparison of the lift and drag performances for the reference foil (Foil “0000”) and its counterpart (Foil “1111”) with a full set of leading-edge tubercles, at a 4m/s inflow velocity which corresponds to the highest Reynolds number that was achieved. Figure 18 clearly shows the beneficial effect of the tubercles on the lift coefficient and hence on the lift-to-drag ratios. It is interesting to note in Figure 18 that the lift coefficients of both foils are almost identical up to an angle of attack (AOA) of 9-10° after which Foil “1111” can maintain a linear growth until 16° AOA while Foil “0000” cannot. This results in a 32% increase of the lift-to-drag ratio for the foil with leading-edge tubercles compared to the reference foil, as shown in Figure 19. Meanwhile the peak lift-to-drag ratio of Foil “1111” also shows a 5.8% higher value at 4° AOA. From Figure 19, it is clear that the enhancement caused by the leading-edge tubercles can be observed over the majority of the range of AOAs tested.

3.3.3 Performance Tests with Different Tubercle Coverage Arrangements

Although the beneficial effect of leading-edge tubercles covering the whole span of the foil has been confirmed in the previous section, it has been reported in other research that this effect may vary depending on the position and extent of the tubercles’ coverage relative to the foil span [18]. Therefore 3 different tubercle coverage arrangements, which were described in Section 3.1 as Foil “0001”, “0011”, “0111”, were tested to identify the optimum arrangement. Five sets of tests, which also included the reference foil (“0000”) and the foil with full coverage of tubercles (“1111”), were conducted at 3m/s and the results were compared, as shown in Figure 20 to Figure 22. From the plots of the lift coefficients, it can be seen that the peak lift coefficient tends to increase with the extent of the tubercles. As shown in Figure 20, Foil “1111”, demonstrates the highest lift with a value of 1.48 at 16° AOA. Nevertheless this arrangement also displays the highest drag. Based on the comparisons of the lift-to-drag ratios of the tested arrangements, it appears that Foil “0001”, which had 1/4 of its leading-edge covered with tubercles, displayed an overall better performance. This can be clearly seen in Figure 21 and Figure 22 where Foil “0001” shows a positive impact from 0° to 26° AOA with more than 10% enhancement in the maximum lift-to-drag ratio at 5° AOA, compared to the reference (Foil “0000”). Even though Foil “1111” displayed the highest growth rate at 16° AOA, Foil “0001” may offer more potential in improving the performance of a tidal turbine operating over a wider range of tip speed ratios.

3.4 Flow Visualization Results and Analysis

3.4.1 Mapping the Flow Separation Region

Flow visualization tests with Foil “0000” and Foil “1111” were performed at a 3 m/s tunnel inflow speed and at AOAs of 16° and 24°. For these conditions, the flow fields across three selected sections along the foil span were visualised using the PIV device. The locations of the selected sections are shown in Figure 23 for Foil “1111” and these positions were repeated for Foil “0000”. For each test condition, 100 pairs of PIV images were analysed and averaged to achieve the time-averaged data. The images of the flow fields and associated velocity vectors at the three selected sections are shown in Table 3 and Table 4 for the AOA of 16° and 24°, respectively.

Firstly, concentrating on the 16° AOA results in Table 3, as shown in the first column (Section1) the flow separation observed at the back of Foil “1111” is much stronger than the separation observed at the back of Foil “0000”. As the visualisation sections are getting closer to the foil tip the flow separation gradually vanishes as shown in the flow field results for “Section2” and “Section3”. This can be related to the strong rolling up effect of the tip vortex forming from the pressure side to the suction side of the foil which would reduce the flow separation. In fact, hardly any flow separation could be observed from the results of “Section2” and “Section3” with Foil “0000”.

On the other hand, as shown in Table 4, the results of the flow visualisations at 24° AOA indicate severe flow separation for both foils. However the separation experienced by Foil “1111” was even more severe than that experienced by Foil “0000”.

3.4.2 Development of Tip Vortex Cavitation

Perhaps the most striking difference between the flow pattern around Foil “0000” and Foil “1111”, was the development of a very strong tip vortex cavitation generated by Foil “0000” as opposed to almost no such cavitation generated by Foil “1111” due to the effect of the leading-edge tubercles. This can be clearly seen in the results given in Table 3 for the test condition with a 3m/s incoming velocity and 16° AOA. A close-up of this cavitating vortex, which emanated from the tip of the reference foil with about a 10mm diameter, is shown in Figure 24.

Using a typical cavitating Rankine vortex expression, the relationship between the diameter of the cavitating tip vortex, a_c , and its circulation, Γ , can be given by Equation 3 [25].

$$p_\infty - p_v = \frac{0.5\rho\Gamma^2}{4\pi^2 a_c^2} \quad \text{Equation (3)}$$

where, p_∞ is the pressure in far field and p_v is the saturated vapour pressure of the water.

According to Equation 3, the larger the diameter is, the stronger the vorticity. Since both foils were tested under the same conditions, the larger tip vortex cavitation experienced by the reference foil would be responsible for the stronger “end effect” and hence greater loss of lift. whereas its counterpart (Foil “1111”) with the leading-edge tubercles would maintain the 2D flow by lowering the end effect and therefore experience more favourable lift characteristics for the same condition.

3.4.3 Concluding Remarks on the Effect of Leading-Edge Tubercles

Based on the observations and analyses so far, by combining our understandings from the flow analysis with regard to the effect of different grades of flow separation and that of tip cavitation generation with and without leading-edge tubercles, we can conclude that the leading-edge tubercles can effectively weaken the 3 dimensional effect of the hydrofoil.

This hypothesis has been firstly supported by the evidence of much weaker separations observed on the back of the reference foil with the smooth leading edge compared to the much more severe separations observed on the counterpart foil with the leading-edge tubercles. Since

the measuring sections are very close to the tip, the 3D effect generates the rolling up flow which can reduce the flow separation close to the tip region. Therefore the more severe the flow separation at the tip region is, the weaker the 3D effect is.

On the other hand the hypothesis was also complemented by the evidence of suppressed tip vortex cavitation and hence much reduced vortex strength resulting from the leading-edge tubercles. This also supported that the 3D effect was weakened by the leading-edge tubercles.

4 Conclusions

This paper reports research into the design, optimization and validation of a tidal turbine blade to exploit the potential benefits of biomimetics in the form of leading-edge tubercles. Based on the research so far, the following conclusions can be drawn:

1. As demonstrated in the optimisation study based on the 2D foil, while the application of leading-edge tubercles could maintain high lift coefficients under post-stall conditions, it could also lower the magnitude of the maximum lift. Based on the optimisation study, a sinusoidal form of leading-edge tubercle profile with $0.1C$ height and $0.5C$ wavelength appeared to be a good compromise for an optimum design and this was applied on a 3D foil which was model tested to validate its performance.
2. Comparative model tests of the 3D foil with a smooth leading edge (no tubercles) and with the leading tubercles, which covered the whole span of the foil, confirmed the significant benefits of the tubercles on the lift and lift-to-drag ratio of the foil despite a slight increase in the drag characteristics. A maximum improvement of 32% in C_L/C_D can be gained in the post stall region at a 16° of angle of attack due to the linear increase of the lift coefficient maintained with the increase of the angle of attack.
3. By optimising the application length of the leading-edge tubercles along the foil span, it was found that the maximum lift coefficient was reduced with the reduced tubercle application length. However, due to the enhanced lift coefficients before the stall and compromised increase in the drag coefficient, the foil with the shortest tubercle application length, which was equal to a $1/4$ of the span, at the tip region displayed the best overall performance amongst the different combinations tested. This was based on the increased lift-to-drag coefficient ratio over the wider range of angles of attack and more than 10% increase in the peak lift-to-drag ratio.
4. The flow visualisations of the 3D foil with and without the leading-edge tubercles indicated that the strong tip vortex caused by the well-known end effect can be reduced dramatically by the application of the tubercles which maintain the 2 dimensional characteristics of the flow around the 3D foil.

Based on this research, the biomimetic exploitation of tubercles on tidal turbine blades has been shown to be promising. However further fundamental research investigating the tubercle concept and a thorough investigation on tidal turbine models are necessary.

Acknowledgments

This research is funded by the School of Marine Science and Technology, Newcastle University and China Scholarship Council. Hence the financial support obtained from both establishments is gratefully acknowledged. The Authors would like to thank all the team members in the Emerson Cavitation Tunnel for the help in testing and sharing their knowledge.

Reference

- [1] F.E. Fish, P.W. Weber, M.M. Murray, L.E. Howle, The tubercles on humpback whales' flippers: application of bio-inspired technology, *Integrative and comparative biology*, 51 (2011) 203-213.
- [2] Frank E. Fish, J.M. Battle, Hydrodynamic design of the humpback whale flipper, *Journal of Morphology*, (1996).
- [3] K. L. Hansen, R. M. Kelso, B.B. Dally, The effect of leading edge tubercle geometry on the performance of different airfoils, (2009).
- [4] H.S. Yoon, P.A. Hung, J.H. Jung, M.C. Kim, Effect of the wavy leading edge on hydrodynamic characteristics for flow around low aspect ratio wing, *Computers & Fluids*, 49 (2011) 276-289.
- [5] H. Johari, C. Henocho, D. Custodio, A. Levshin, Effects of leading-edge protuberances on airfoil performance, *Aiaa J*, 45 (2007) 2634-2642.
- [6] D.S. Miklosovic, M.M. Murray, L.E. Howle, Experimental evaluation of sinusoidal leading edges, *J Aircraft*, 44 (2007) 1404-1408.
- [7] M.J. Stanway, Hydrodynamic effects of leading-edge tubercles on control surfaces and in flapping foil propulsion, in, *Massachusetts Institute of Technology*, 2008.
- [8] P.W. Weber, L.E. Howle, M.M. Murray, Lift, drag, and cavitation onset on rudders with leading-edge tubercles, *Mar Technol Sname N*, 47 (2010) 27-36.
- [9] A. Corsini, G. Delibra, A.G. Sheard, On the role of leading-edge bumps in the control of stall onset in axial fan blades, *J Fluid Eng-T Asme*, 135 (2013) 081104-081104.
- [10] T. Swanson, K.M. Isaac, Biologically Inspired Wing Leading Edge for Enhanced Wind Turbine and Aircraft Performance, in, *AIAA*, 2011.
- [11] E. van Nierop, S. Alben, M. Brenner, How bumps on whale flippers delay stall: An aerodynamic model, *Physical Review Letters*, 100 (2008).
- [12] L. Bellequant, L.E. Howle, Whalepower wenvor blade, (2009).
- [13] K.L. Hansen, R.M. Kelso, B.B. Dally, Performance variations of leading-edge tubercles for distinct airfoil profiles, *Aiaa J*, 49 (2011) 185-194.

- 420 [14] D.C.a.L.M. Mark W. Lohry, Characterization and Design of Tubercle Leading-Edge Wings,
421 in: Seventh International Conference on Computational Fluid Dynamics (ICCFD7), Big Island,
422 Hawaii, 2012.
- 423 [15] J.H. Chen, S.S. Li, V.T. Nguyen, The effect of leading edge protuberances on the
424 performance of small aspect ratio foils.
- 425 [16] G. Sisinni, D. Pietrogiaconi, G.P. Romano, Biomimetic wings, *Advances in Science and*
426 *Technology*, 84 (2012) 72-77.
- 427 [17] D.S. Miklosovic, M.M. Murray, L.E. Howle, F.E. Fish, Leading-edge tubercles delay stall on
428 humpback whale (*Megaptera novaeangliae*) flippers, *Phys Fluids*, 16 (2004) L39-L42.
- 429 [18] T. Gruber, M.M. Murray, D.W. Fredriksson, Effect of humpback whale inspired tubercles
430 on marine tidal turbine blades, in: *ASME 2011 International Mechanical Engineering Congress*
431 *and Exposition*, American Society of Mechanical Engineers, 2011, pp. 851-857.
- 432 [19] D. Wang, M. Atlar, R. Sampson, An experimental investigation on cavitation, noise, and
433 slipstream characteristics of ocean stream turbines, *Proceedings of the Institution of*
434 *Mechanical Engineers, Part A: Journal of Power and Energy*, 221 (2007) 219-231.
- 435 [20] D.M. Somers, Design and experimental results for the S814 airfoil, in, *National Renewable*
436 *Energy Laboratory, NREL/SR-440-6919 • UC Category: 1213 • DE97000104*, 1997.
- 437 [21] J. Janiszewska, R.R. Ramsay, M. Hoffmann, G. Gregorek, Effects of grit roughness and
438 pitch oscillations on the S814 airfoil, in, *National Renewable Energy Lab., Golden, CO (United*
439 *States)*, 1996.
- 440 [22] F. Menter, M. Kuntz, R. Langtry, Ten years of industrial experience with the SST
441 turbulence model, *Turbulence, heat and mass transfer*, 4 (2003) 625-632.
- 442 [23] ANSYS, Release 14.5 Documentation, Inc ANSYS, (2013).
- 443 [24] M. Atlar, Recent upgrading of marine testing facilities at Newcastle University, in:
444 *AMT'11, the second international conference on advanced model measurement technology*
445 *for the EU maritime industry*, 2011, pp. 4-6.
- 446 [25] J.B.W. McCormick, On Cavitation Produced by a Vortex Trailing From a Lifting Surface,
447 *Journal of Fluids Engineering*, 84 (1962) 369-378.

448

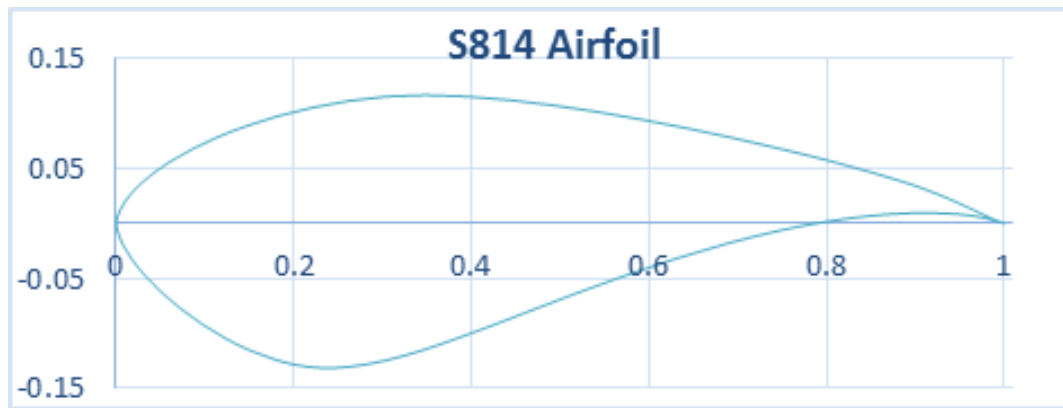


Figure 1 Cross-section profile of S814 [19]



Figure 2 Scaled tidal turbine model mounted on the dynamometer of Emerson Cavitation Tunnel [19]

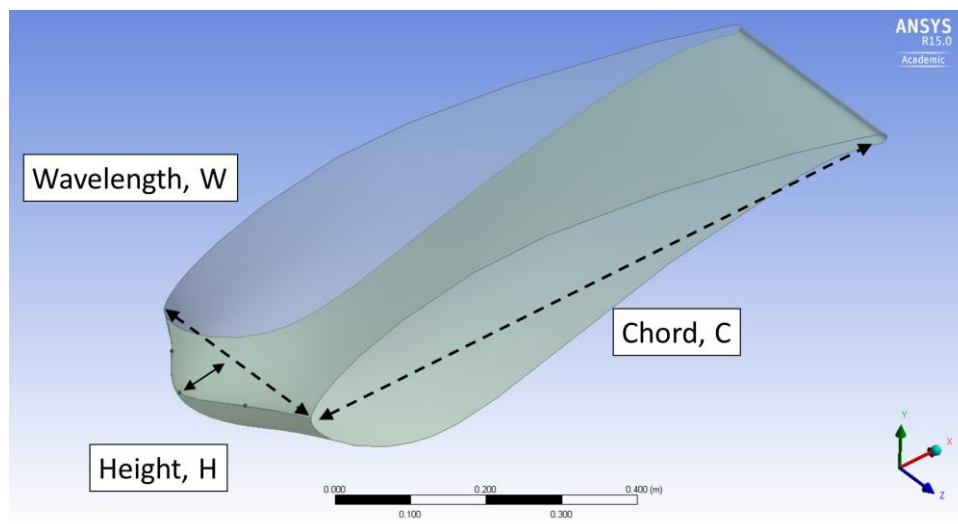


Figure 3 Definition of 2D foil with a sinusoidal tubercle

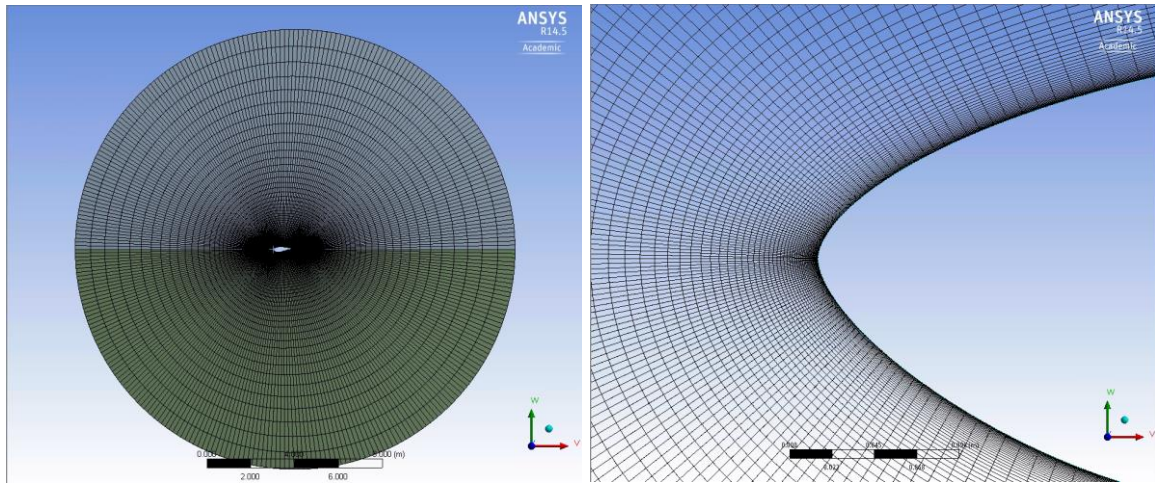


Figure 4 Mesh overview (left) and zoom-in view of wing section at the leading edge (right)

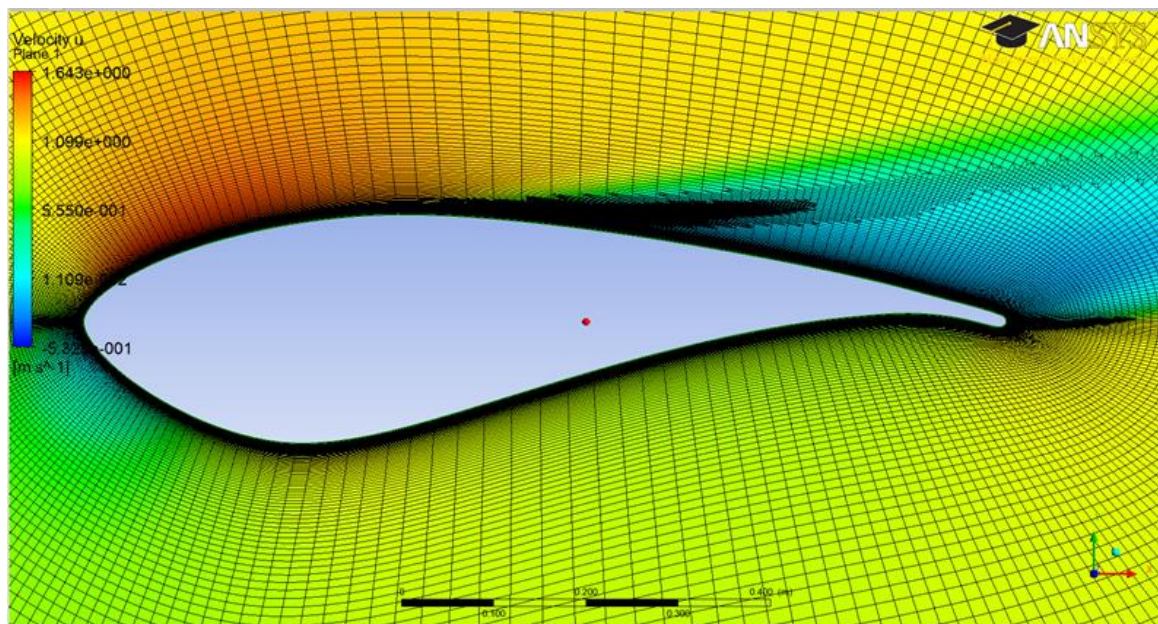


Figure 5 Refined mesh by the “solution adaptive mesh” method

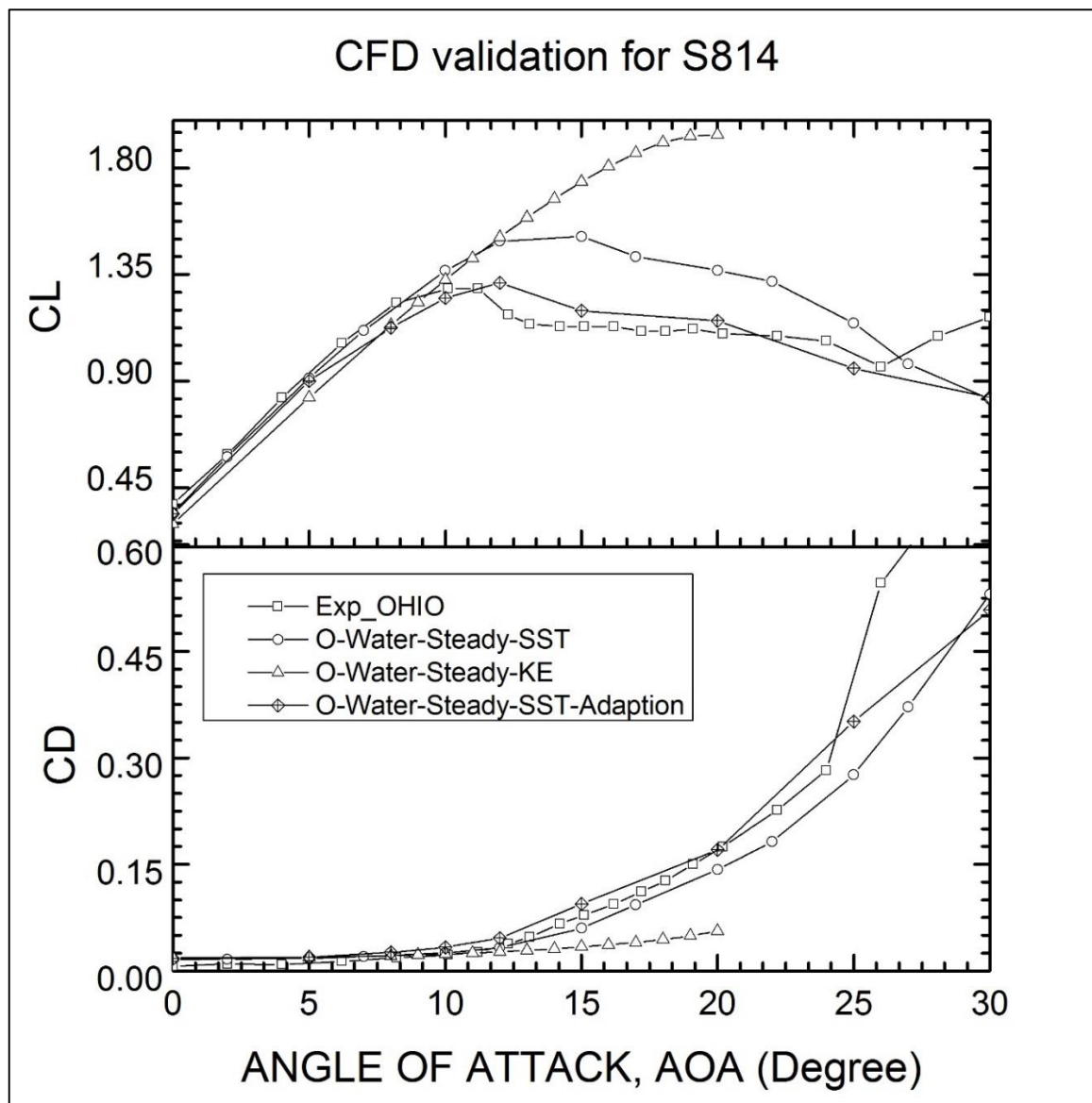


Figure 6 Validation for CFD prediction of lift and drag coefficients of S814 airfoil

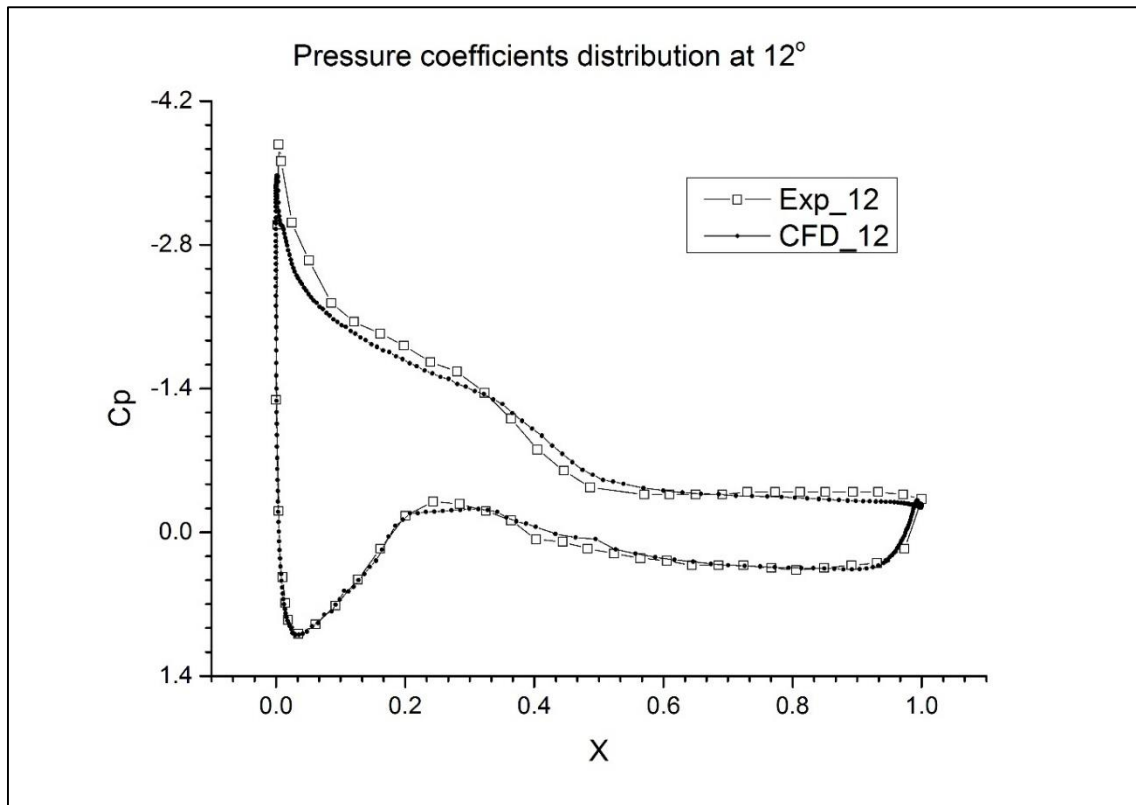


Figure 7 Validation for CFD prediction of Pressure coefficient distribution at 12° of angle of attack

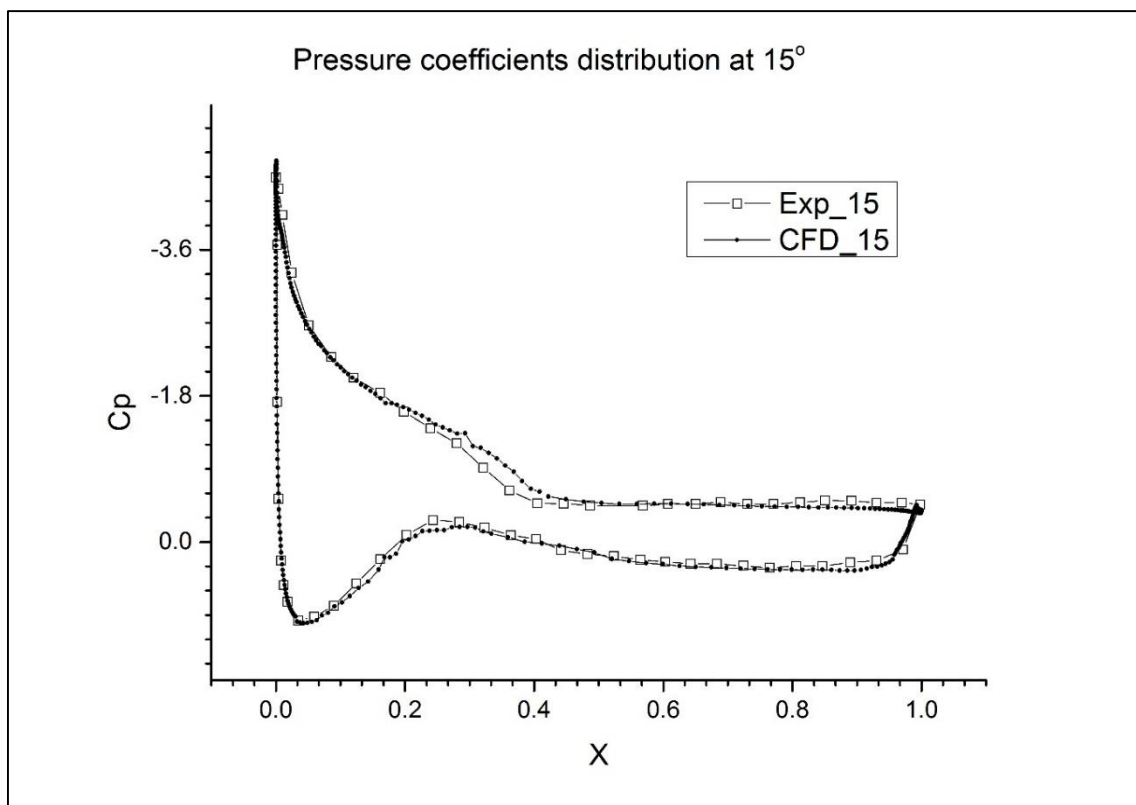


Figure 8 Validation for CFD prediction of Pressure coefficient distribution at 15° of angle of attack

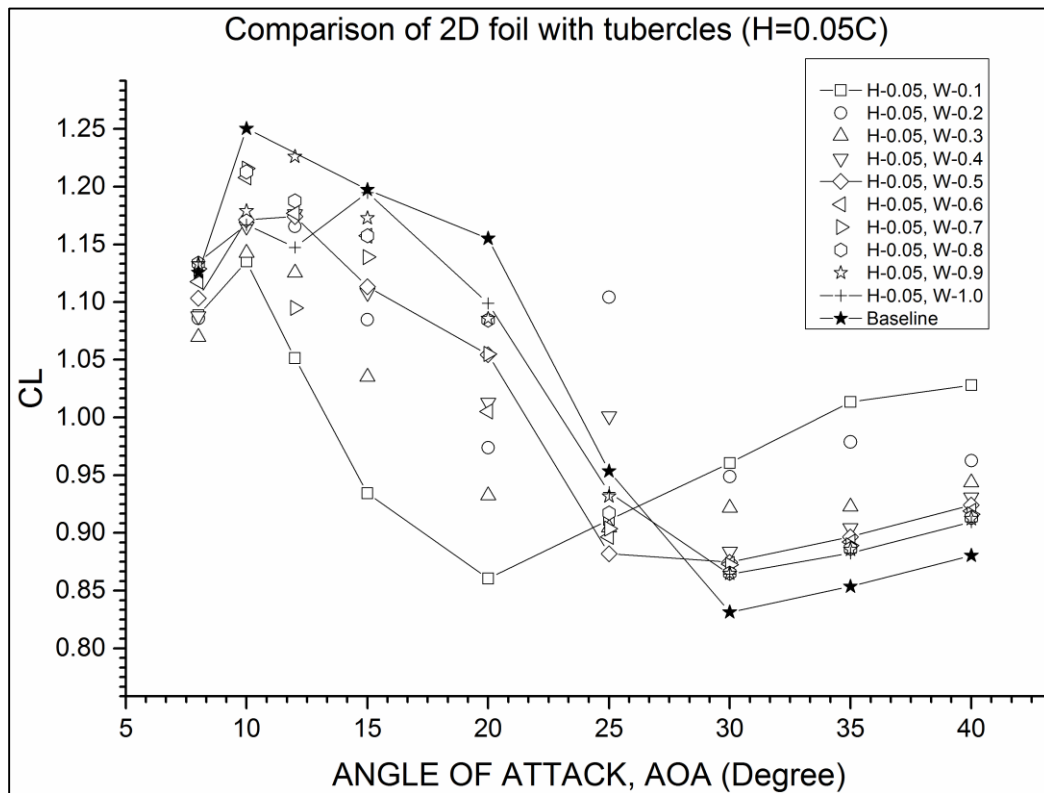


Figure 9 Comparison of 2D foil lift coefficients with different tubercle profiles by varying the wavelength (W) at constant tubercle height ($H=0.05C$)

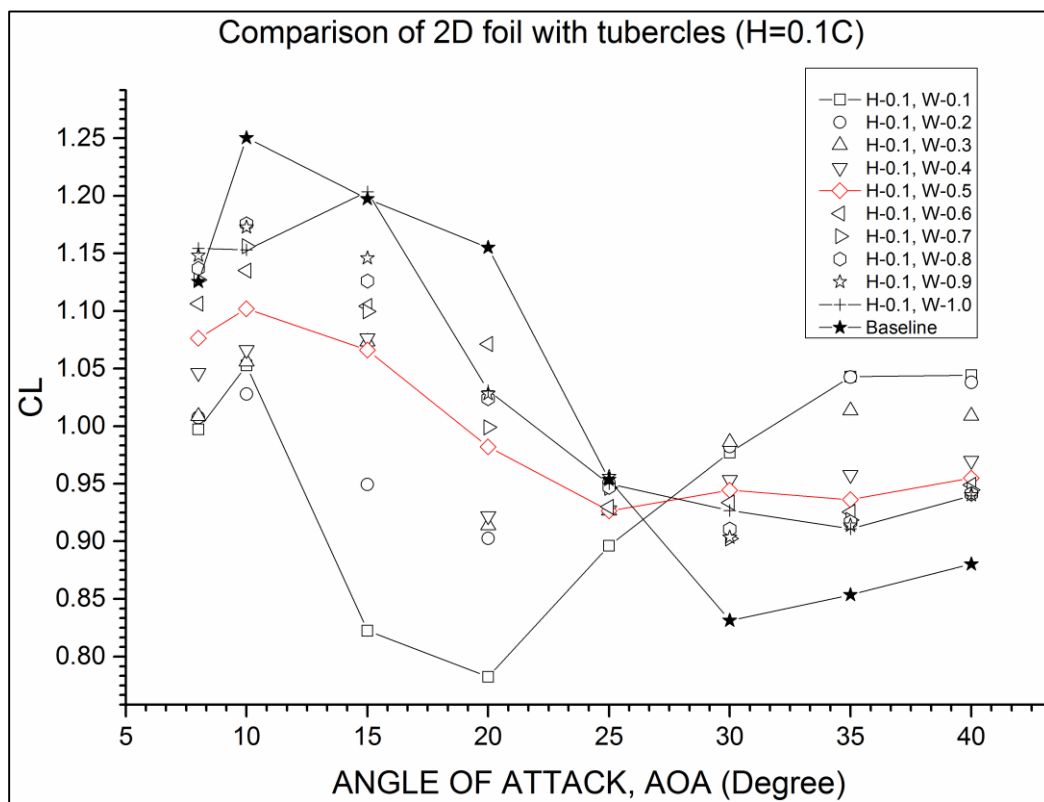
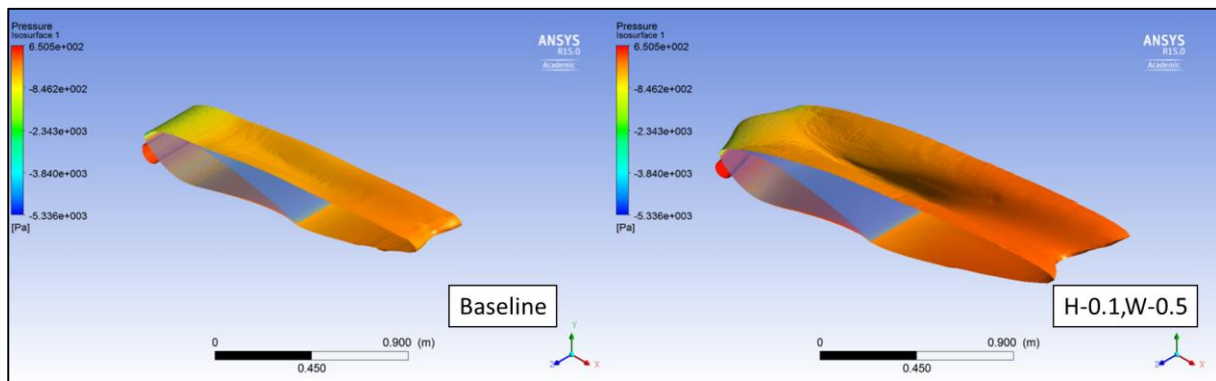


Figure 10 Comparison of 2D foil lift coefficients with different tubercle profiles by varying the wavelength (W) at constant tubercle height ($H=0.1C$)

471

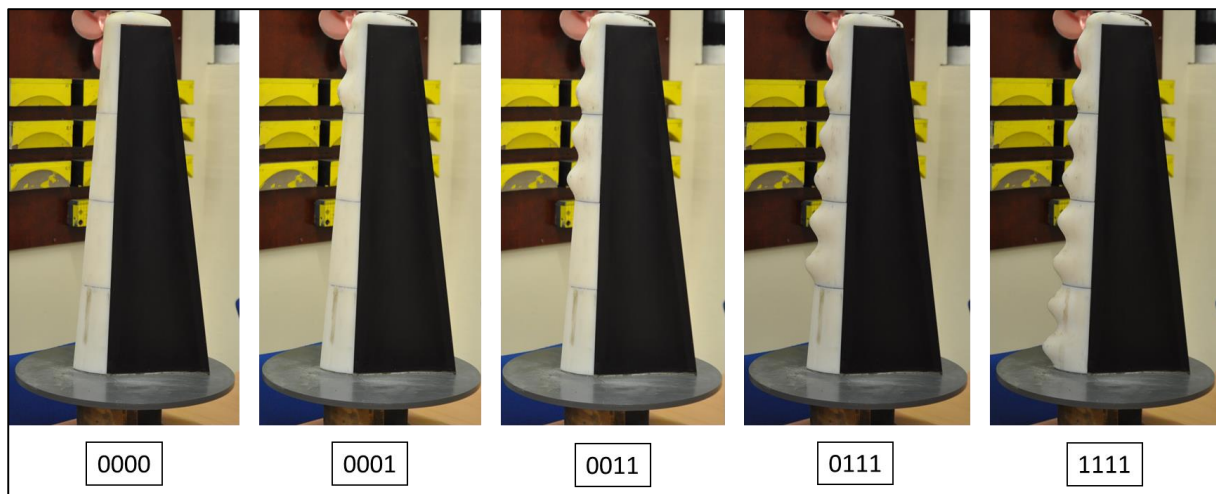


472

473

474

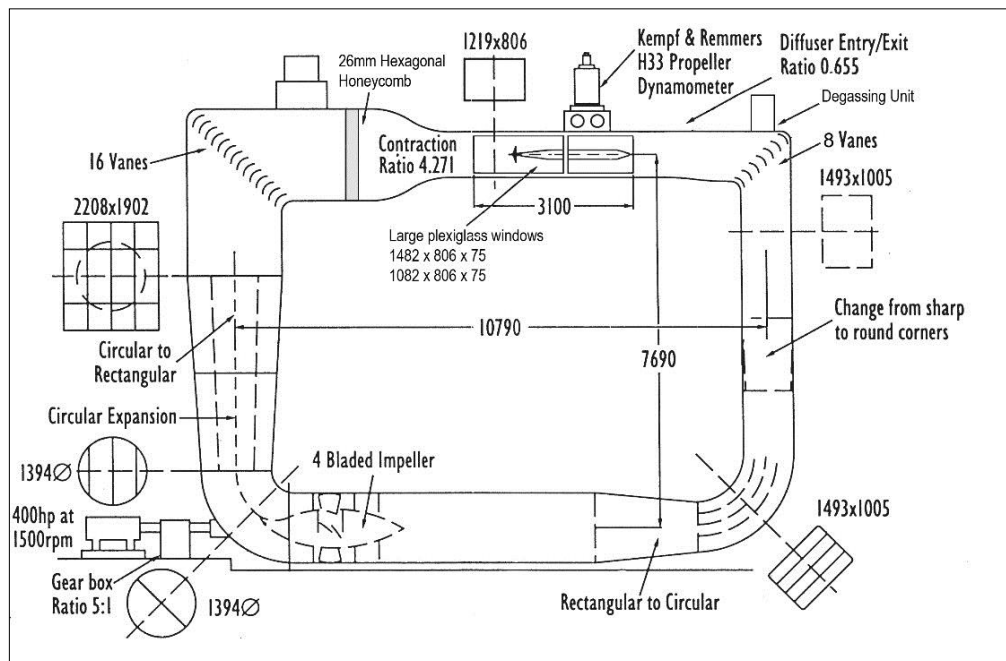
Figure 11 Comparison of flow separation at 15° angle of attack (Velocity isosurface at 50% of incoming velocity coloured by pressure distribution)



475

476

Figure 12 Tested 3D hydrofoil models with interchangeable leading-edge parts



477

478

Figure 13 Sketch of the Emerson Cavitation Tunnel

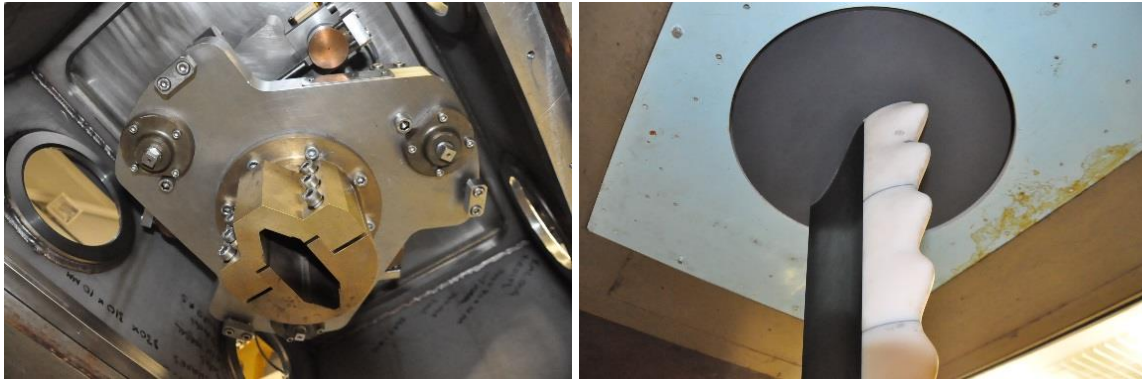


Figure 14 Setup of 3-component balance (Cussons R102) on the Emerson Cavitation Tunnel upper lid (Left) and setup of tested foil mounted on the 3-component balance (right)

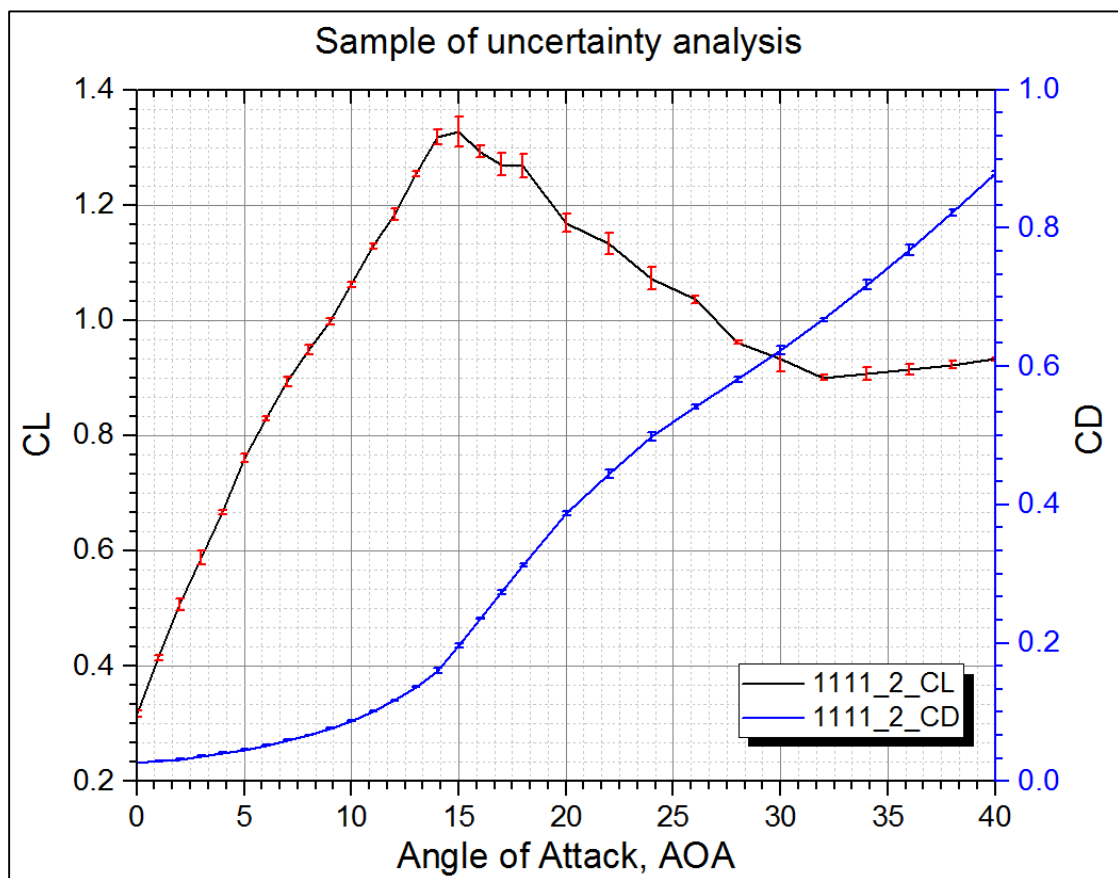


Figure 15 Sample of uncertainty analysis results applied on the measured lift and drag coefficients

Reynolds number effect on "0000"

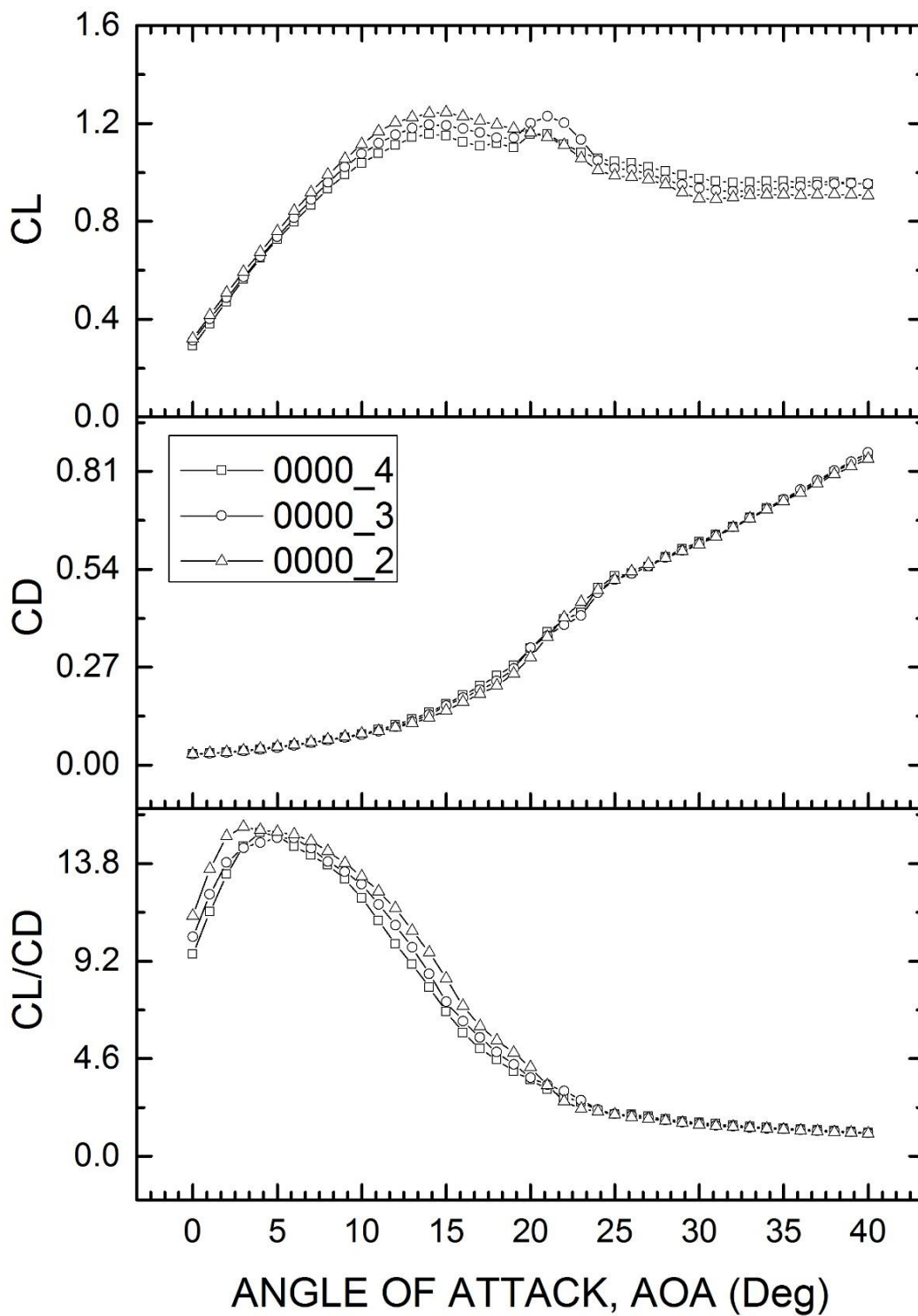


Figure 16 Experimental data for Foil "0000" with smooth leading edge at different incoming velocities

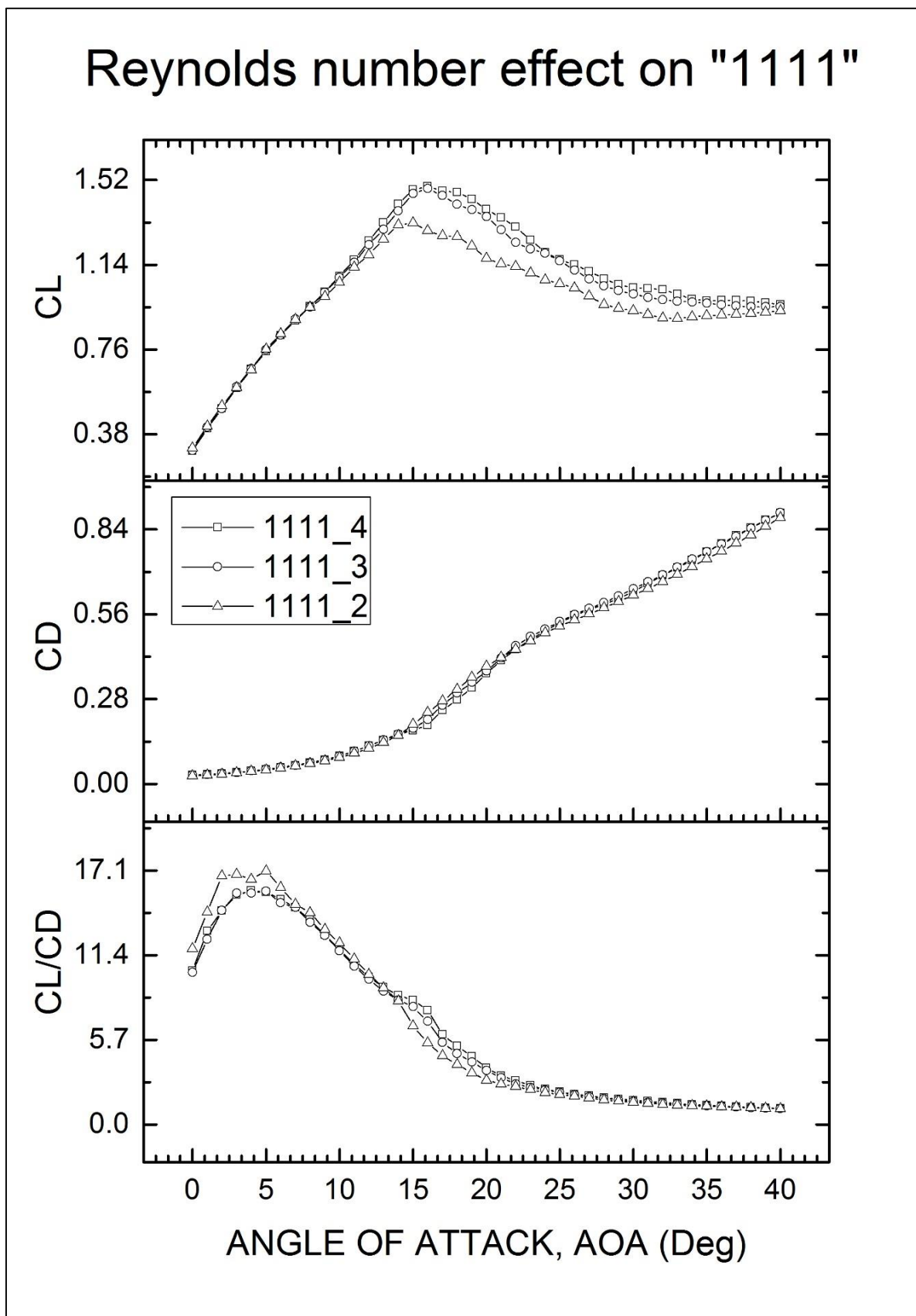


Figure 17 Experimental data for Foil "1111" with leading-edge tubercles at different incoming velocity

Comparison between "1111" and "0000"

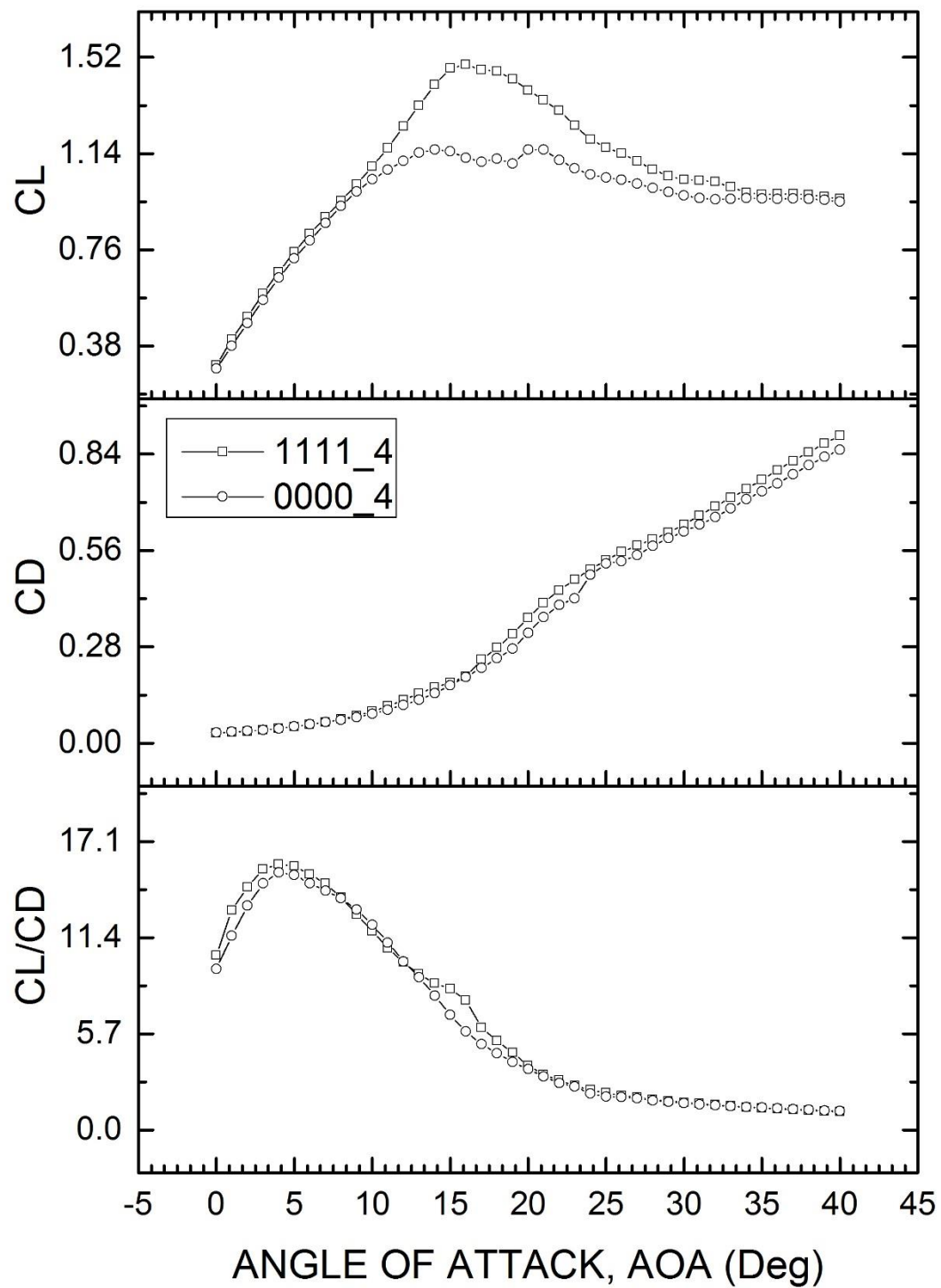


Figure 18 Comparison of experimental data for Foil "0000" and Foil "1111" at 4m/s

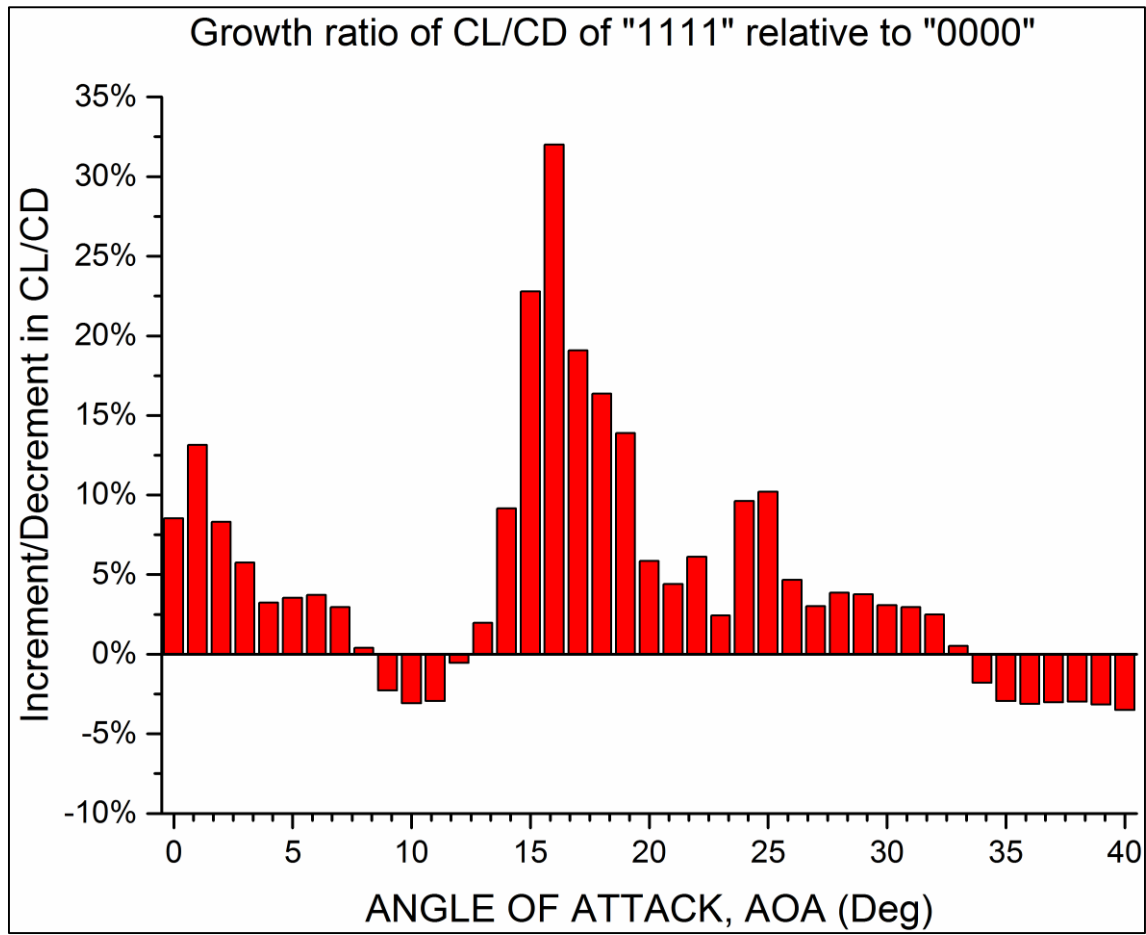


Figure 19 Growth ratio of C_L/C_D for Foil "1111" (with leading-edge tubercles) relative to Foil "0000" (with smooth leading edge)

Comparison of different configurations

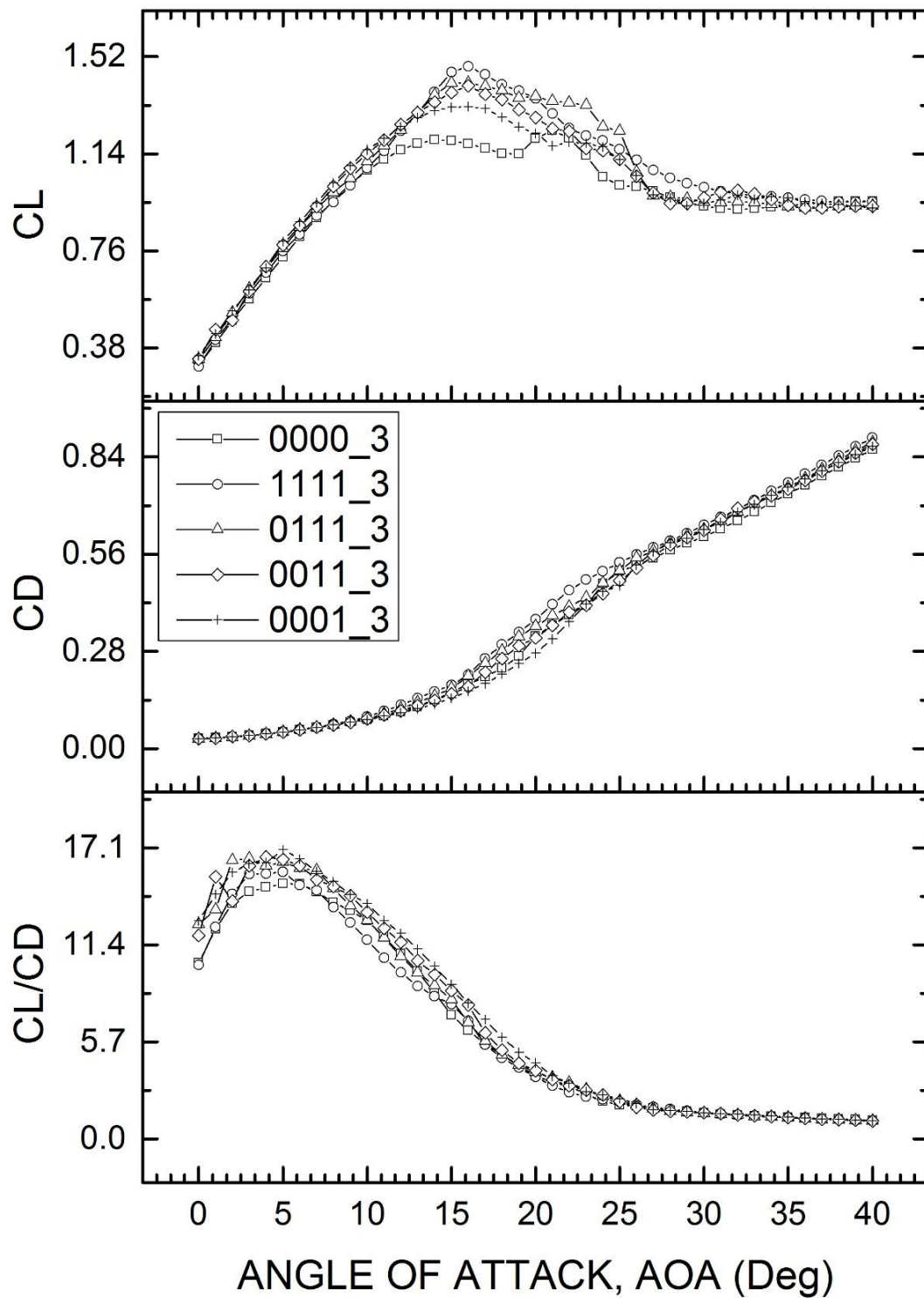


Figure 20 Comparison of experimental data for different leading-edge tubercle coverage arrangements

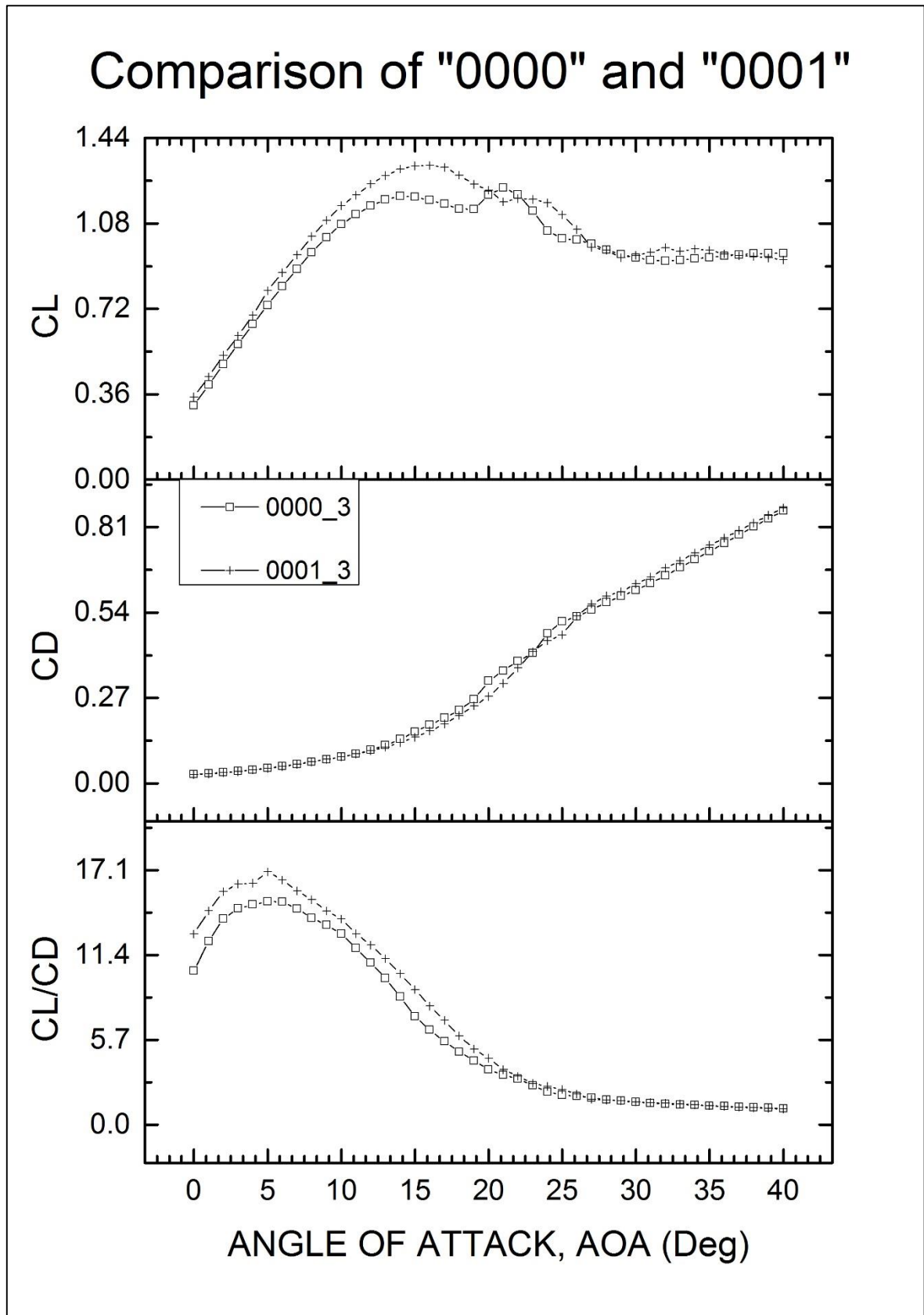


Figure 21 Comparison of experimental data for foil with minimum leading-edge tubercle coverage ("0001") and for the reference foil ("0000") at 3m/s.

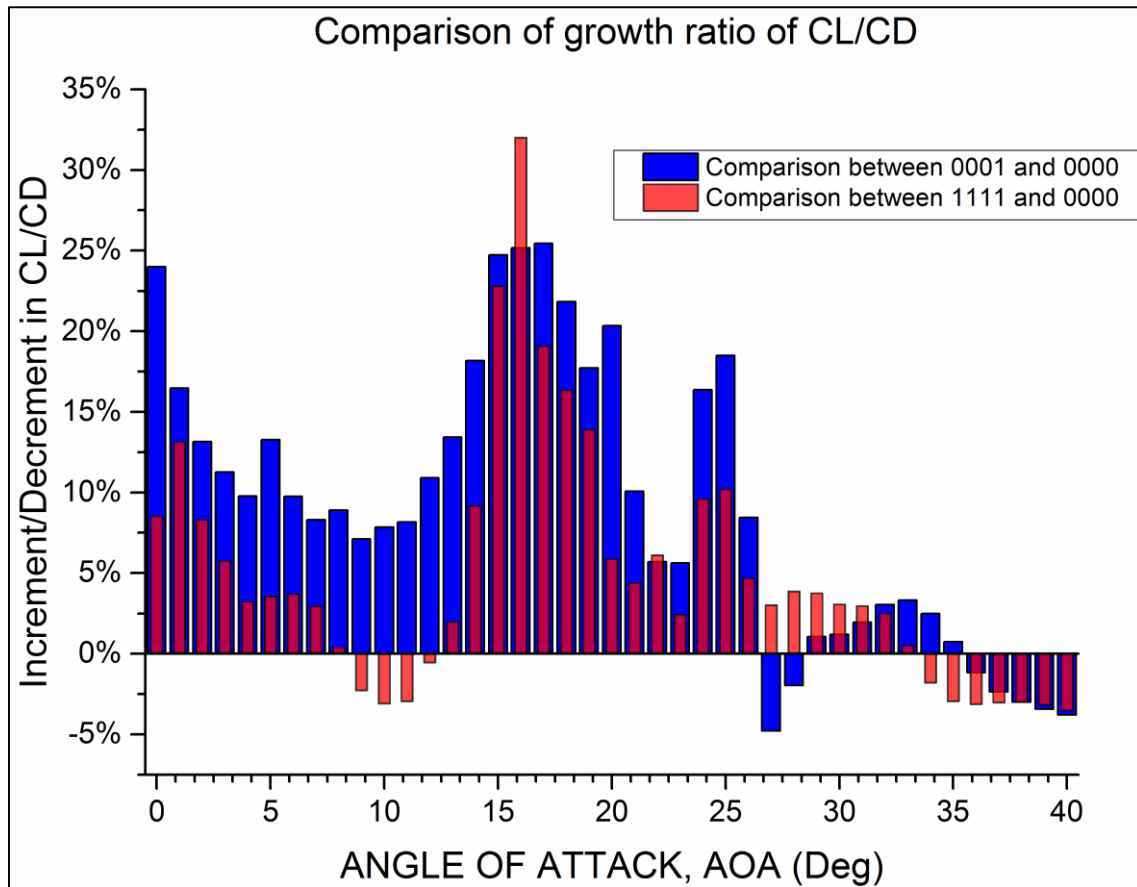


Figure 22 Comparison of relative growth ratios for C_L/C_D for Foil “1111” (with leading-edge tubercles applied on whole span) and Foil “0001” (with minimum leading-edge tubercles applied around the tip)

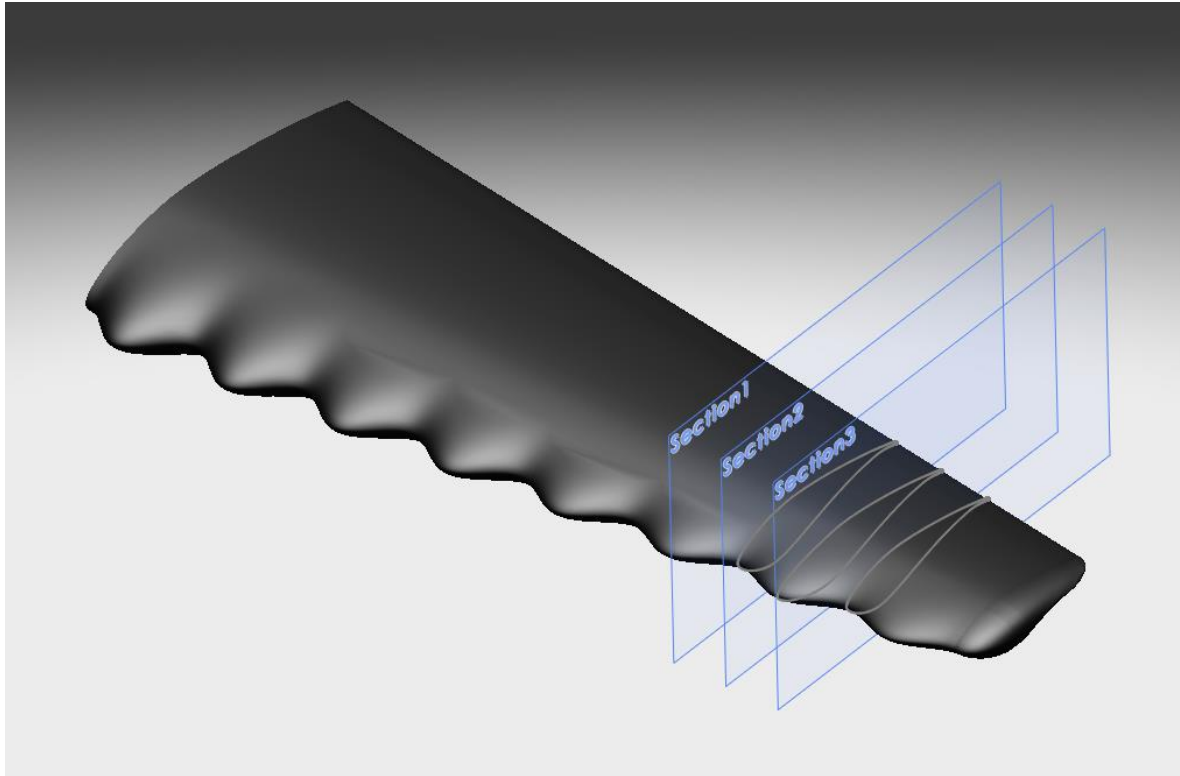


Figure 23 Sectional positions selected along Foil “1111” for flow visualization using PIV

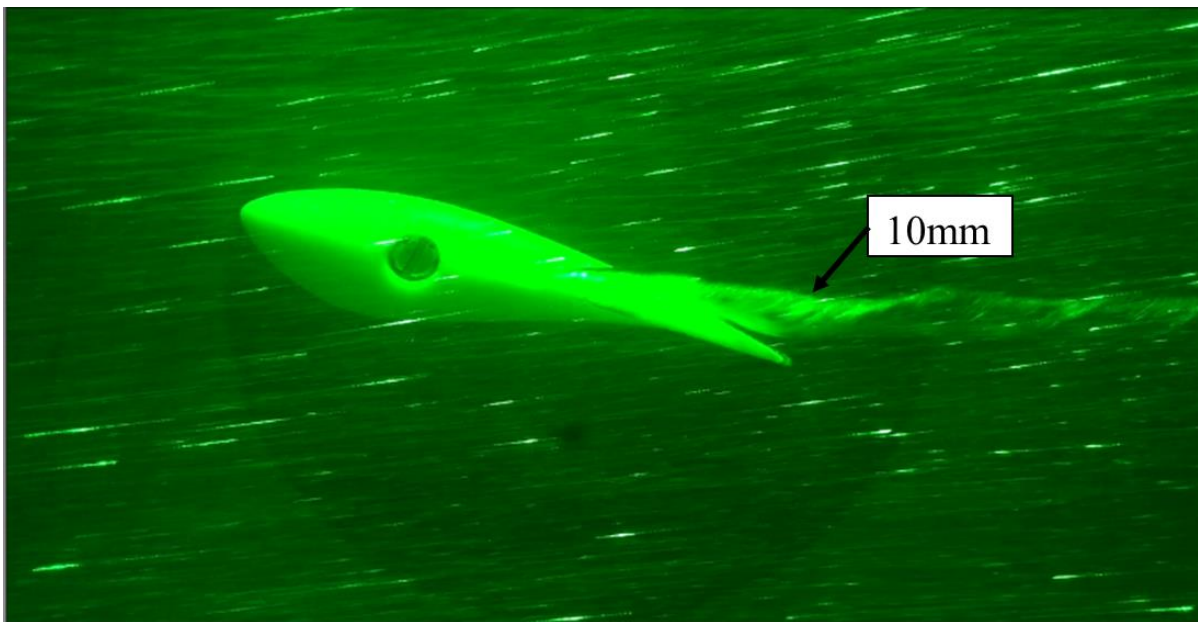


Figure 24 Cavitating tip vortex observation on reference foil with smooth leading edge
(Note a 10mm diameter tip vortex cavitation was generated)

508

Table 1 Chord distribution of the reference foil

Span(mm)	0	70	140	210	280	350	420	490	560
Chord(mm)	225.1	210.08	195.06	180.04	165.02	150	134.98	119.96	104.94

509

510

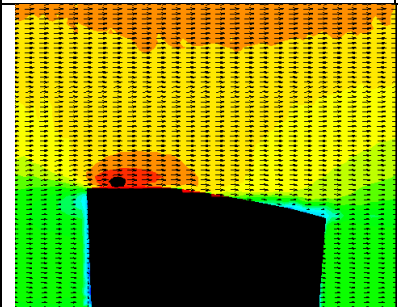
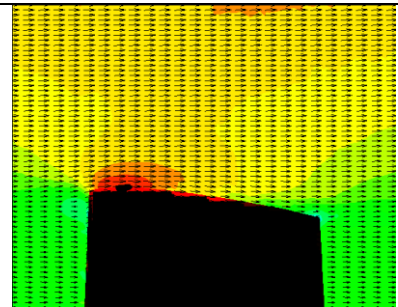
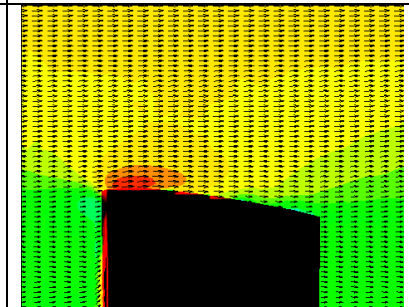

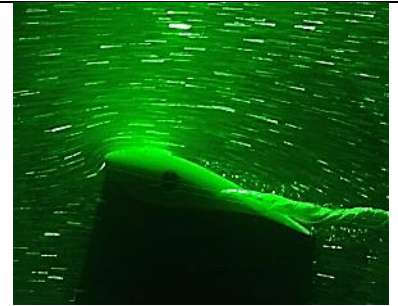
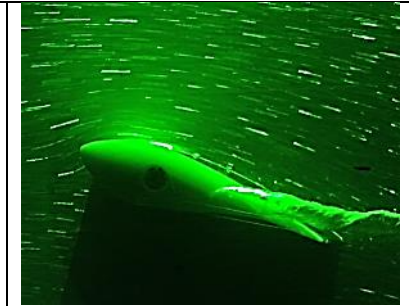
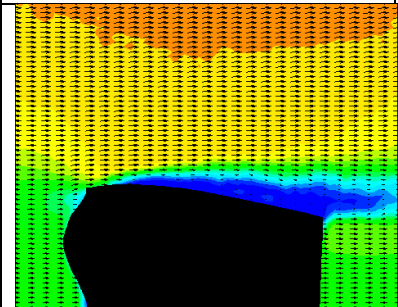
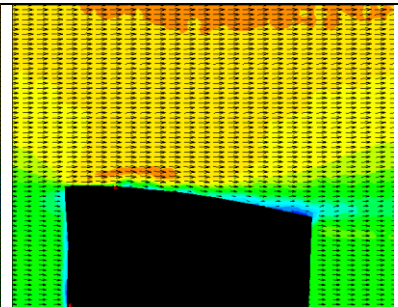
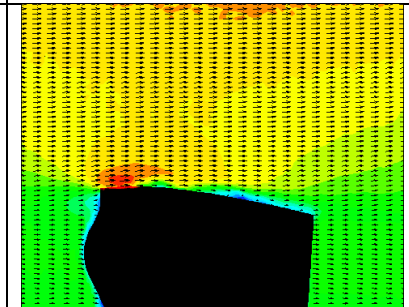


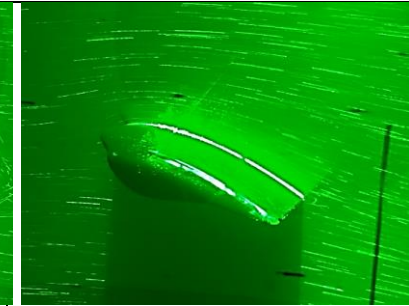
Table 2 Specifications of Dantec Dynamics Stereo PIV (Particle Image Velocimetry) system

Laser	NewWave Pegasus
Wavelength	527nm
Repetition rate per head	1-10K Hz; 2-20K Hz
Energy –Dual Cavity System	10 mJ @ 2000 Hz
Light sheet optics	80x70 high power Nd:YAG light sheet series
Synchronizer	NI PCI-6601 timer board
Camera	NanoSense MK III
Sensor size	1280x1024 pixels
Maximum capture frequency	1000Hz
Maximum images	3300
Seeding particles	Talisman 30 white 110 plastic powder

511

512
513

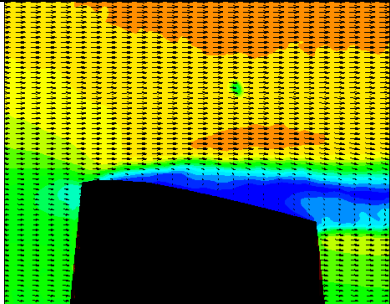
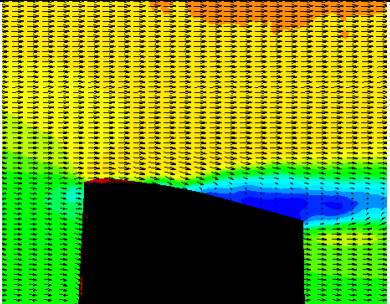
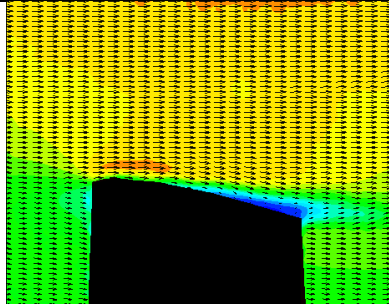



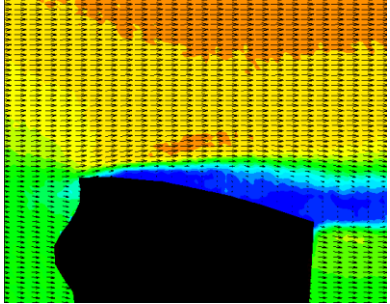
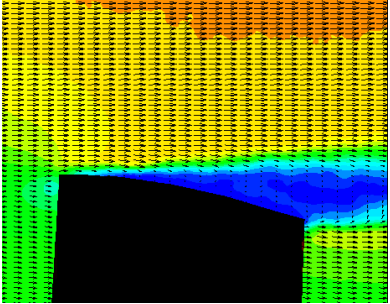
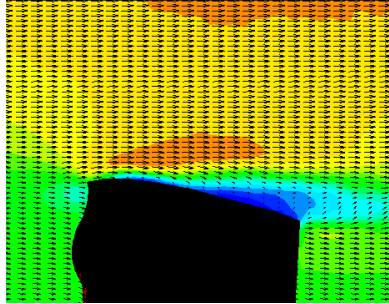



Table 3 Comparative experimental flow patterns at 3 selected sections for Foil “0000” and Foil “1111” observed at 16° of angle of attack

“0000”, foil with smooth leading edge		
Section 1	Section 2	Section 3
		
		
“1111”, foil with leading-edge tubercles		
Section 1	Section 2	Section 3
		
		

514

515
516

Table 4 Comparative experimental flow patterns at 3 selected sections for Foil “0000” and Foil “1111” observed at 24° of angle of attack

“0000”, foil with smooth leading edge		
Section 1	Section 2	Section 3
		
		
“1111”, foil with leading-edge tubercles		
Section 1	Section 2	Section 3
		
		

517